Mathematical Biosciences and Engineering

MBE, 20(9): 15544–15567.
DOI: 10.3934/mbe.2023694
Received: 11 April 2023
Revised: 20 June 2023
Accepted: 29 June 2023
Published: 27 July 2023

http://www.aimspress.com/journal/MBE

Research article

Mechanical behavior of an FGM-type frozen soil wall: Theory and numerical analysis

Qinglong Wang[1], Han Wang[2], Junyuan Zhang[2,*], Dongyang Wu[1] and Ruliang Zhao[3]

[1] Yunnan Laman Expressway Co., Ltd. Xishuangbanna 666300, China
[2] School of Highway, Chang'an University, Xi'an 710064, China
[3] Bei Fang Investigation, Design & Research Co., Ltd. Tianjin 300223, China

* **Correspondence:** Email: xianzjy@chd.edu.cn; Tel: +8615129022557.

Abstract: With a laminate model foundation, we have used the complex variable function method to calculate the boundary displacement and stress of a frozen soil wall in a horizontal connecting passage. Using an actual engineering case, the effects of the number of divided layers of a functionally graded material-type frozen soil wall, the position of the freezing pipe and the section shape of the connecting passage on the displacements and tangential stresses of the frozen soil wall are discussed. The results indicate that the frozen soil wall as a temporary support structure exhibits a good supporting effect. With the increase of layers, the material strength of the frozen soil wall weakens, and the displacements and tangential stresses of the inner boundary increase. When the midline of the freezing pipe moves toward the inner boundary, the tensile area in the frozen soil wall begins to shift, and the displacements and tangential stresses of the inner boundary decrease differently. Thedistributions of internal boundary displacements and tangential stresses are significantly affected by the section shape of the frozen soil wall, and the internal boundary displacements and tangential stresses of the frozen soil wall of the small section are more uniform than those of the frozen soil wall of the large section.

Keywords: tunnel; connecting passage; frozen soil wall; complex variable function method; functionally graded material; laminated model

1. Introduction

With the rapid development of urban mass transit technology and the increasing demand for transportation, the artificial ground freezing method is widely used in the construction of connecting passagesbecause of its characteristics including the exclusion of water, pressure bearing capability lack of pollution and flexibility [1–3]. Currently, the design of a horizontal connecting passage frozen soil wall is still in the semi-empirical and semi-theoretical stage, and it is mainly analyzed by means of a numerical method, model testing and in-situ monitoring [4–7]. In contrast to a shaft, the shape of the cross section of the communication channel isnot a standard circular ring and is instead an irregular shape similar to a straight-wall arch; thus, the mechanical behavior analysis of the frozen soil wall is more complicated. Sokolnikoff [8] first used the complex variable function method to deal with the plane strain problem associated with a complex hole in an infinite domain, and many scholars subsequently began using an analytical continuation solution, the Cauchy integration solution, a power series solution, and other solutions to examine the aforementioned problem with different hole shapes [9–11]. The complex variable function method was introduced to solve the problem of surrounding rock-mass stress distribution in an elastic zone owing to the excavation of various buried tunnels without support, and it was studied in detail, ranging from simple circular tunnels to rectangular tunnels and straight-wall arch tunnels among others [12–16]. Lu [17–20] began mapping the irregular tunnel into a circular section conformally for analysis.

Specifically, the frozen soil wall is not an ideal homogeneous structure; it is composed of artificial frozen soil, and its material strength is gradually graded along with the temperature from the ceter to the outside of the frozen soil wall. This type of composite material with material strength gradient is generally referred to as a functionally graded material (FGM). Hence, existing studies [21–24] assumed that the modulus of elasticity of the shaft material varies radially in different nonlinear forms, such as the exponential function and power function, and they derived closed form solutions for an FGM thick cylinder. The studies indicated that the FGM thick cylinder can undergo plastic deformation in a manner entirely different from its homogeneous counterpart. This observation led to immense interest in the area of civil engineering. Several researchers [25–29] proposed substituting the soil mechanic's calculation method for FGM thick cylinders with the non-homogeneous solution of the frozen soil wall by assuming that the relationship between the strength of the frozen soil wall and the temperature field are trapezoidal and parabolic.

Given the irregular section shape and material heterogeneity of the frozen soil wall, mechanical behavior analysis of the frozen soil wall of a horizontal connecting passage can be very complicated. Previous soil mechanic's calculation methods considered limited factors, and rarely associated the temperature field with the deformation of the frozen soil wall. Given the gradient effect of the strength of frozen soil, the current study combines a laminate model with the complex function method to analyze the behavior of the frozen soil wall a of horizontal connecting passage and establishes a new method to derive an analytical solution of boundary stress and boundary displacement.

2. Mechanical model

2.1. Assumptions

In order to calculate the stress and displacement of a frozen soil wall of a horizontal connecting passage, the following assumptions are made:

1) In any cross section of the frozen soil wall, it is considered as a straight-wall arch that is similar to the outer contour of the connecting passage, and the cross section near the center of the connecting passage is considered as the standard section.

2) We ignore the gradient of the frozen interface caused by the oblique installation of the freezing pipes, and the cross section of the frozen soil wall of the connecting passage is considered as continuous and consistent in the direction perpendicular to the axis of the shield tunnel.

3) The frozen soil wall is completely frozen and ignores the effect of the frost heaving force imposed on the frozen soil wall [30].

4) The main influence area of the single-row multi-pipe layout is a limited part in the middle of the adjacent freezing pipes. The temperature distribution outside of the influence area can be described as a logarithmic function of the radial distance.

2.2. Conformal transformation of straight-wall arch section

A simple ring-shaped region in the ζ plane (Figure 1) can be conformally transformed into a complicated frozen soil wall across the section in the Z plane (Figure 2) and its mapping function $\omega(\zeta)$ satisfies the Laurent series as follows:

$$z = \omega(\zeta) = R(\zeta + \sum_{k=0}^{n} C_k \zeta^{-k}) \tag{1}$$

where R denotes a positive real number representing the size of the ring; C_k denotes the shape correction coefficient; z denotes the complex potential coordinate of the Z plane; ζ denotes the complex potential of the ζ plane.

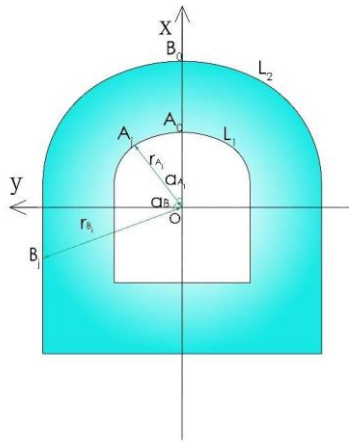

Figure 1. Original shape of the frozen soil wall (Z plane).

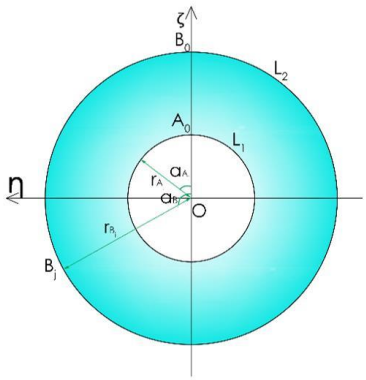

Figure 2. Mapping shape of the frozen soil wall (ζ plane).

Using the complex method to solve the mapping function $\omega(\zeta)$, a new optimization function is constructed as follows:

$$f = \sum_{j=1}^{m_1}(r_{A_j} - f_{A_j})^2 + \sum_{j=1}^{m_2}(r_{B_j} - f_{B_j})^2 \tag{2}$$

where f denotes the optimization function; r_{Aj} and r_{Bj} are known as the polar coordinate values of the Z plane; f_{Aj} and f_{Bj} denote the polar coordinate values of the Z plane obtained from the mapping function.

When the function f is minimized, the corresponding C_k^* denotes the solution that satisfies the following constraints:

$$\sum_{k=1}^{n} k|C_k| < 1 \tag{3}$$

where k denotes a positive integer.

2.3. Stress and displacement field of frozen soil wall

According to the complex variable function theory [21–23,31] the equations of the stress components and displacement components at any point (in polar coordinates in the Z plane) in the frozen soil wall are expressed as follows:

$$\begin{cases} \sigma_\theta + \sigma_r = 4\,Re[\,\Phi(\zeta)] \\ \sigma_\theta - \sigma_r + 2i\tau_{\theta r} = \frac{2\zeta^2}{r^2\omega'(\zeta)} \times [\overline{\omega(\zeta)}\Phi'(\zeta) + \omega'(\zeta)\Psi(\zeta)] \\ 2G(u_r + iu_\theta) = \frac{\overline{\zeta\omega'(\zeta)}}{r|\omega'(\zeta)|} \times [\kappa\varphi(\zeta) - \frac{\omega(\zeta)}{\overline{\omega'(\zeta)}} \times \overline{\varphi'(\zeta)} - \overline{\psi(\zeta)}] \end{cases} \tag{4}$$

where σ_θ, σ_r, and $\tau_{\theta r}$ denote the tangential, radial and shear stresses, respectively; u_θ and u_r denote the tangential and radial displacements, respectively; K denotes the plane strain, K = 3–4μ; G denotes the shear modulus; μ denotes Poisson's ratio; $\varphi(\zeta)$, $\psi(\zeta)$, $\Phi(\zeta)$, and $\Psi(\zeta)$ are the analytic functions, as given by the following equations:

$$\begin{cases} \varphi(\zeta) = \varphi_j(z) = \varphi_j[\omega(\zeta)] \\ \psi(\zeta) = \psi_j(z) = \psi_j[\omega(\zeta)] \\ \Phi(\zeta) = \varphi_j'(z) = \frac{\varphi'(\zeta)}{\omega'(\zeta)} \\ \Psi(\zeta) = \psi_j'(z) = \frac{\psi'(\zeta)}{\omega'(\zeta)} \end{cases} \tag{5}$$

where j denotes the serial number of the ring layer, and j=n+1 denotes the serial number of the surrounding rock.

We exclude the weight of the soil in the frozen soil wall, and the initial stress field is expressed as follows:

$$\begin{cases} \sigma_r^0 = -\frac{1+\lambda}{2}p - \frac{\lambda-1}{2}p \times \left\{ \left[\mathrm{Re}\left(\frac{\bar{\zeta}\overline{\omega'(\zeta)}}{r|\omega'(\zeta)|} \right) \right]^2 - \left[\mathrm{Im}\left(\frac{\bar{\zeta}\overline{\omega'(\zeta)}}{r|\omega'(\zeta)|} \right) \right]^2 \right\} \\ \sigma_\theta^0 = -\frac{1+\lambda}{2}p + \frac{\lambda-1}{2}p \times \left\{ \left[\mathrm{Re}\left(\frac{\bar{\zeta}\overline{\omega'(\zeta)}}{r|\omega'(\zeta)|} \right) \right]^2 - \left[\mathrm{Im}\left(\frac{\bar{\zeta}\overline{\omega'(\zeta)}}{r|\omega'(\zeta)|} \right) \right]^2 \right\} \\ \tau_{r\theta}^0 = \frac{\lambda-1}{2}p \times \left\{ 2\,\mathrm{Re}\left(\frac{\bar{\zeta}\overline{\omega'(\zeta)}}{r|\omega'(\zeta)|} \right) \mathrm{Im}\left(\frac{\bar{\zeta}\overline{\omega'(\zeta)}}{r|\omega'(\zeta)|} \right) \right\} \end{cases} \tag{6}$$

where σ_r^0, σ_θ^0 and $\tau_{r\theta}^0$ denote the initial radial, tangential, and shear stresses, respectively; p denotes the vertical earth pressure; λ denotes the lateral pressure coefficient; Re{} denotes the real part of {}; Im denotes the imaginary part of {}.

We combine Eqs (5) and (6) to obtain the analytical solution expressions stress and displacement field of the frozen soil wall and surrounding rock-mass as follows:

$$\begin{cases} \sigma_r = 2\,Re[\frac{\varphi_j'(\zeta)}{\omega'(\zeta)}] - Re\left\{ \frac{\zeta^2}{r^2\overline{\omega'(\zeta)}} \left[\overline{\omega(\zeta)}[\frac{\varphi_j'(\zeta)}{\omega'(\zeta)}]' + \omega'(\zeta)[\frac{\psi_j'(\zeta)}{\omega'(\zeta)}] \right] \right\} - \frac{1}{2}\frac{\lambda+1}{2}p - \frac{\lambda-1}{2}p \left\{ \left[Re\left(\frac{\bar{\zeta}\overline{\omega'(\zeta)}}{r|\omega'(\zeta)|} \right) \right]^2 - \left[Im\left(\frac{\bar{\zeta}\overline{\omega'(\zeta)}}{r|\omega'(\zeta)|} \right) \right]^2 \right\} \\ \sigma_\theta = 2\,Re[\frac{\varphi_j'(\zeta)}{\omega'(\zeta)}] + Re\left\{ \frac{\zeta^2}{r^2\overline{\omega'(\zeta)}} \left[\overline{\omega(\zeta)}[\frac{\varphi_j'(\zeta)}{\omega'(\zeta)}]' + \omega'(\zeta)[\frac{\psi_j'(\zeta)}{\omega'(\zeta)}] \right] \right\} - \frac{1}{2}\frac{\lambda+1}{2}p + \frac{\lambda-1}{2}p \left\{ \left[Re\left(\frac{\bar{\zeta}\overline{\omega'(\zeta)}}{r|\omega'(\zeta)|} \right) \right]^2 - \left[Im\left(\frac{\bar{\zeta}\overline{\omega'(\zeta)}}{r|\omega'(\zeta)|} \right) \right]^2 \right\} \\ \tau_{r\theta} = Im\left\{ \frac{\zeta^2}{r^2\overline{\omega'(\zeta)}} \left[\overline{\omega(\zeta)}[\frac{\varphi_j'(\zeta)}{\omega'(\zeta)}]' + \omega'(\zeta)[\frac{\psi_j'(\zeta)}{\omega'(\zeta)}] \right] \right\} - \frac{\lambda-1}{2}p \left\{ 2\,Re\left(\frac{\bar{\zeta}\overline{\omega'(\zeta)}}{r|\omega'(\zeta)|} \right) Im\left(\frac{\bar{\zeta}\overline{\omega'(\zeta)}}{r|\omega'(\zeta)|} \right) \right\} \\ u_r = Re\left\{ \frac{1}{2G_j}\frac{\overline{\zeta}\overline{\omega'(\zeta)}}{r|\omega'(\zeta)|}[\kappa_j\varphi_j(\zeta) - \frac{\omega(\zeta)}{\overline{\omega'(\zeta)}} \times \overline{\varphi_j'(\zeta)} - \overline{\psi_j(\zeta)}] \right\} \\ u_\theta = Im\left\{ \frac{1}{2G_j}\frac{\overline{\zeta}\overline{\omega'(\zeta)}}{r|\omega'(\zeta)|}\left[\kappa_j\varphi_j(\zeta) - \frac{\omega(\zeta)}{\overline{\omega'(\zeta)}} \times \overline{\varphi_j'(\zeta)} - \overline{\psi_j(\zeta)}\right] \right\} \qquad (j = 1,2\cdots) \end{cases} \tag{7}$$

where G_j denotes the shear modulus of the ring at layer j; k_j denotes the plane strain of the ring at layer j.

2.4. Boundary conditions

We use the continuity of displacements and stresses at the ring boundary, and the equation the boundary stress condition of the inner boundary of the ring is as follows:

$$\varphi_j(t_1) + \frac{\omega(t_1)}{\overline{\omega'(t_1)}}\overline{\varphi_j'(t_1)} + \overline{\psi_j(t_1)} = f(t_1) \tag{8}$$

The boundary conditions of stresses and displacements at the outer ring boundary are as follows:

$$\varphi_j(t_2) + \frac{\omega(t_2)}{\overline{\omega'(t_2)}}\overline{\varphi_j'(t_2)} + \overline{\psi_j(t_2)} = \varphi_{j+1}(t_2) + \frac{\omega(t_2)}{\overline{\omega'(t_2)}}\overline{\varphi_{j+1}'(t_2)} + \overline{\psi_{j+1}(t_2)} \tag{9}$$

$$\frac{\kappa_1}{G_j}\varphi_1(t_2) - \frac{1}{G_j}\left[\frac{\omega(t_2)}{\overline{\omega'(t_2)}}\overline{\varphi_j'(t_2)} + \overline{\psi_j(t_2)}\right] = \frac{\kappa_2}{G_{j+1}}\varphi_2(t_2) - \frac{1}{G_{j+1}}\left[\frac{\omega(t_2)}{\overline{\omega'(t_2)}}\overline{\varphi_{j+1}'(t_2)} + \overline{\psi_{j+1}(t_2)}\right] \tag{10}$$

The boundary condition of displacement at infinity is as follows:

$$\frac{\kappa_2}{G_{n+1}}\varphi_{n+1}(t_3) - \frac{1}{G_{n+1}}\left[\frac{\omega(t_3)}{\overline{\omega'(t_3)}}\overline{\varphi_{n+1}'(t_3)} + \overline{\psi_{n+1}(t_3)}\right] = 0 \tag{11}$$

In Eq (12), based on the Fourier series [12,18], the boundary stresses $f(t_1)$ and $\frac{\omega(t)}{\overline{\omega'(t)}}$ are expanded as follows:

$$\frac{\omega(t)}{\overline{\omega'(t)}} = \sum_{s=-n}^{n} L_s \zeta^s \tag{12}$$

$$f(t_1) = \sum_{s=0}^{\infty} A_s e^{is\theta} + \sum_{s=0}^{\infty} B_s e^{-is\theta} \tag{13}$$

where $t\left(t = \rho e^{i\theta}\right)$ denotes a point (ρ, θ) in the ζ plane; t_1 and t_2 denote the point on the inner boundary of the *j*-layer ring and the point on the outer boundary of the *j*-layer ring, respectively; t_3 denotes a point at infinity; $f(t_1)$ denotes the surface force function; L_s, A_s and B_s denote polynomial coefficients; *i* denotes an imaginary unit; *s* denotes the number of analytical function coefficients.

3. Basic equations for solving analytical functions for an FGM

Indicated that the temperature distribution inside the frozen soil wall approximates the gradient variation, and that the material parameters, such as the strength of the artificial frozen soil, also exhibit a certain functional relationship with temperature. Therefore, the frozen soil wall is a heterogeneous material from the very beginning. Based on the FGM theory, it is considered that the strength of the frozen soil wall changes on a gradient with the internal temperature distribution, and the strength of the artificial frozen soil wall is expressed as follows:

$$G = F[T(r)] = G(r) \tag{14}$$

where *T(r)* denotes the steady-state temperature field; *r* denotes the distance between a point on the Z plane and the freezing pipe.

The mechanical model of an FGM includes the laminated model, among others [32–34]. When thegraded function model cannot be determined directly, the laminate model is the most convenient and feasible method. In the study, the laminated model is applied, and the calculation method is close to the finite difference method: the frozen soil wall is divided into *n* layers along the radial direction, and different strength parameters (shear module) are assigned to the n-layer frozen soil wall as determined by the steady temperature field. We then calculate the stress-related analytic functions for each layer step by step to derive its stresses and displacements.

Analytic functions of the j layer frozen soil wall are as follows:

$$\begin{cases} \varphi_j(\zeta) = \sum_{s=1}^{n} a_s \zeta^s + \sum_{s=1}^{n} b_s \zeta^{-s} \\ \psi_j(\zeta) = \sum_{s=0}^{n} c_s \zeta^s + \sum_{s=0}^{n} d_s \zeta^{-s} \end{cases} \tag{15}$$

Analytic functions of the j+1 layer frozen soil wall are as follows:

$$\begin{cases} \varphi_{j+1}(\zeta) = \sum_{s=1}^{n} a_s' \zeta^s + \sum_{s=1}^{n} b_s' \zeta^{-s} \\ \psi_{j+1}(\zeta) = \sum_{s=0}^{n} c_s' \zeta^s + \sum_{s=0}^{n} d_s' \zeta^{-s} \end{cases} \tag{16}$$

Analytic functions of the surrounding rock-mass （n+1 layer） are as follows:

$$\begin{cases} \varphi_{n+1}(\zeta) = \sum_{s=1}^{n} g_s \zeta^{-s} \\ \psi_{n+1}(\zeta) = \sum_{s=0}^{n} h_s \zeta^{-s} \end{cases} \tag{17}$$

where a_s, b_s, c_s, d_s, a_s', b_s', c_s', d_s', g_s and h_s denote the to be solved.

We substitute Eqs (15)–(17) into the boundary conditions to yield the stress outer boundary conditions in the jth layer (j = 1,2,3, ..., n-1):

$$\begin{cases} b_n + \sum_{s=1}^{n} sL_{s-n-1} a_s r_j^{2(s-1)} - \sum_{s=1}^{n} sL_{-s-n-1} b_s r_j^{-2(s+1)} + c_n r_j^{-2n} \\ = b_n' + \sum_{s=1}^{n} sL_{s-n-1} a_s' r_{j+1}^{2(s-1)} - \sum_{s=1}^{n} sL_{-s-n-1} b_s' r_{j+1}^{-2(s+1)} + c_n' r_{j+1}^{-2n} \\ a_m + \sum_{s=1}^{m} sL_{s+m-1} a_s r_j^{2(s-1)} - \sum_{s=1}^{m} sL_{-s-m-1} b_s r_j^{-2(s+1)} + d_m r_j^{-2m} \\ = a_m' + \sum_{s=1}^{m} sL_{s+m-1} a_s' r_{j+1}^{2(s-1)} - \sum_{s=1}^{m} sL_{-s-m-1} b_s' r_{j+1}^{-2(s+1)} + d_m' r_{j+1}^{-2m}, \quad (n = 0,1,2,\ldots), (m = 1,2,\ldots) \end{cases} \tag{18}$$

Outer boundary conditions for displacement in the jth layer are as follows:

$$\begin{cases} \frac{\kappa_1}{G_j} b_n - \frac{1}{G_j}\left[\sum_{s=1}^{n} sL_{s-n-1} a_s r_j^{2(s-1)} - \sum_{s=1}^{n} sL_{-s-n-1} b_s r_j^{-2(s+1)}\right] \\ \quad - \frac{1}{G_j} c_n r_j^{-2n} = \frac{\kappa_1}{G_{j+1}} b_n' - \frac{1}{G_{j+1}} \times \\ \left[\sum_{s=1}^{n} sL_{s-n-1} a_s' r_{j+1}^{2(s-1)} - \sum_{s=1}^{n} sL_{-s-n-1} b_s' r_{j+1}^{-2(s+1)}\right] - \frac{1}{G_{j+1}} c_n' r_{j+1}^{-2n} \\ \frac{\kappa_1}{G_j} a_m - \frac{1}{G_i}\left[\sum_{s=1}^{m} sL_{s+m-1} a_s r_j^{2(s-1)} - \sum_{s=1}^{m} sL_{-s-m-1} b_s r_j^{-2(s+1)}\right] \\ \quad - \frac{1}{G_j} d_m r_j^{-2m} = \frac{\kappa_1}{G_{j+j}} a_m' - \frac{1}{G_{j+1}} \times \\ \left[\sum_{s=1}^{m} sL_{s+m-1} a_s' r_{j+1}^{2(s-1)} - \sum_{s=1}^{m} sL_{-s-m-1} b_s' r_{j+1}^{-2(s+1)}\right] - \frac{1}{G_{j+1}} d_m' r_{j+1}^{-2m} \end{cases} \tag{19}$$

Inner boundary stress conditions for the nth layer are as follows:

$$\begin{cases} b_n + \sum_{s=1}^{n} sL_{s-n-1} a_s r_{n-1}^{2(s-1)} - \sum_{s=1}^{n} sL_{-s-n-1} b_s r_{n-1}^{-2(s+1)} + c_n r_{n-1}^{-2n} = B_n r_{n-1}^{n} \\ a_m + \sum_{s=1}^{m} sL_{s+m-1} a_k r_{n-1}^{2(s-1)} - \sum_{s=1}^{m} kL_{-s-m-1} b_s r_{n-1}^{-2(s+1)} + d_m r_{n-1}^{-2m} = A_m r_{n-1}^{-m} \end{cases} \tag{20}$$

Outer boundary conditions for stress in the *n*th layer are as follows:

$$\begin{cases} b_n + \sum_{s=1}^{n} sL_{s-n-1}a_s - \sum_{s=1}^{n} sL_{-s-n-1}b_s + \\ c_n = g_n - \sum_{s=1}^{n} sL_{-s-n-1}g_s, \\ a_m + \sum_{s=1}^{m} sL_{s+m-1}a_s - \sum_{s=1}^{m} sL_{-s-m-1}b_s + \\ d_m = \hbar_m - \sum_{s=1}^{m} sL_{-s-m-1}g_s. \end{cases} \tag{21}$$

Outer boundary conditions for displacement in the *n*th layer are as follows:

$$\begin{cases} \frac{\kappa_1}{G_n} b_n - \frac{1}{G_n}[\sum_{s=1}^{n} sL_{s-n-1}a_s - \sum_{s=1}^{n} sL_{-s-n-1}b_s] \\ -\frac{1}{G_n} c_n = \frac{\kappa_1}{G_{n+1}} g_n + \frac{1}{G_{n+1}} \sum_{s=1}^{n} sL_{-s-n-1}g_s \\ \frac{\kappa_1}{G_n} a_m - \frac{1}{G_n}[\sum_{s=1}^{m} sL_{s+m-1}a_s - \sum_{s=1}^{m} sL_{-s-m-1}b_s] \\ -\frac{1}{G_n} d_m = -\frac{1}{G_{n+1}} \hbar_m + \frac{1}{G_{n+1}} \sum_{s=1}^{m} sL_{-s-m-1}g_s \end{cases} \tag{22}$$

Boundary conditions for displacement at infinity are as follows:

$$\begin{cases} \frac{\kappa_2}{G_{n+1}} g_n + \frac{1}{G_{n+1}} \sum_{s=1}^{n} sL_{-s-n-1}g_s = 0 \\ \frac{1}{G_{n+1}} \hbar_m - \frac{1}{G_{n+1}} \sum_{s=1}^{m} sL_{-s-m-1}g_s = 0 \end{cases} \tag{23}$$

We combine Eqs (18)–(23) to obtain the analytic functions of the *n*th layer to the first layer from the outside to the inside in order.

4. Analysis of engineering case

Processes of solving the stress and displacement of each point in the frozen soil wall of the connecting passage have been divided into three steps The first step involves solving the conformal mapping function. The second step involves using the boundary conditions to derive the analytic function for each layer of the frozen soil wall. In the third step, the analytic function for each layer is substituted into the stress and displacement fields of the frozen soil wall and surrounding rock mass to obtain stress–displacement solutions.

4.1. Project overview

There are two sections in the tunnel of Xiguan cross, i.e., the Dongfanghong square cross of Lanzhou Metro line 1. The first type corresponds to a "narrow long" straight-wall arch section with a pumping station (hereafter referred to as "large section", as below), whose aspect ratio (h/b) is 1.37; The second type corresponds to a standard section ("small section") which has an aspect ratio (h/b) of 1.05. The shape and size of each type of section are shown in Figure 3.

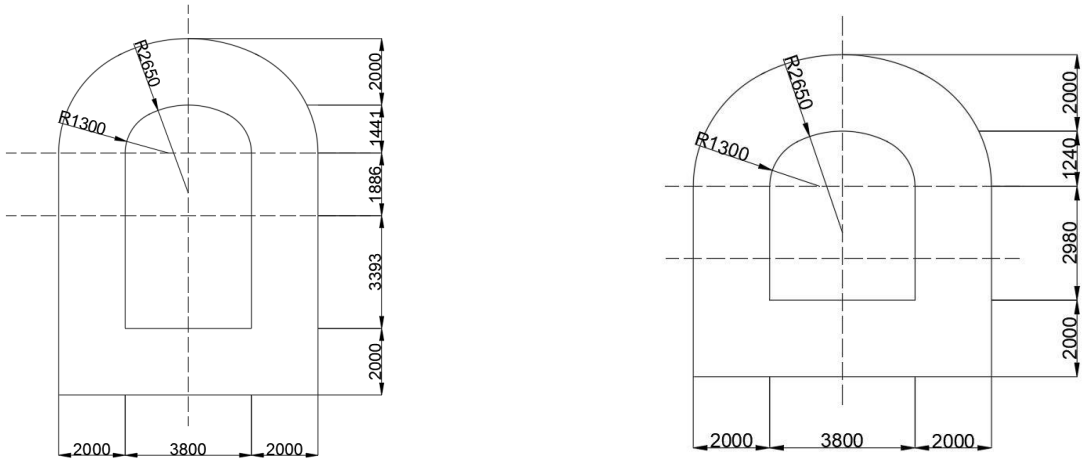

(a) (b)

Figure 3. Dimensions of the frozen soil wall (unit: mm): (a) large section (b) small section.

Regarding the design, the external surface temperature of the freezing pipe corresponds to –28 ℃, the outer boundary temperature of the frozen soil wall corresponds to 0 ℃, the thickness of the frozen soil wall corresponds to 2 m, the radius of the freezing pipe corresponds to 0.127 m, the ultimate tensile strength of the frozen soil at 0 ℃ corresponds to 0.99 MPa and the ultimate compressive strength corresponds to 3.47 MPa. The stratigraphic parameters are listed in Tables 1 and 2 as obtained from the geological survey and on-site measured results.

Table 1. Formation parameters.

Type of soil layer	Thickness （m）	Density (g/cm^3)	Elastic modulus E (MPa)	Internal friction angle φ (°)	Cohesion c (kPa)	Poisson's ratio μ
Miscellaneous fill	3.7	1.90	5.0	15	8	0.39
Plain fill	1.0	1.98	5.5	18	10	0.38
Pebble	4.1	2.30	55.0	40	0	0.16
Sandstone	42.0	2.05	38.0	32	24	0.23

Table 2. Frozen soil wall parameters.

Thickness （m）	μ_{n+1}	K_1	K_2	G_{n+1}/MPa	λ	p/MPa
0.2	0.3	2.2	1.8	15.4	0.65	0.287

In the above table K denotes the plane strain, K=3-4μ; μ denotes Poisson's ratio; G denotes the strength of the artificial frozen soil wall; λ denotes the lateral pressure coefficient; p denotes the vertical earth pressure.

4.2. Process of solving for the conformal mapping function

When the composite method was used to map the circular section to the straight-wall arch section, 20 initial points were uniformly selected on the inner and outer boundaries of the frozen soil wall. A Matlab calculation program was compiled to solve the conformal mapping function.

The large-section frozen soil wall conformal mapping function is as follows:

$$z = \omega(\zeta) = 4.1625(\zeta + 0.1965 + 0.1062\zeta^{-1} - 0.0095\zeta^{-2} - 0.0046\zeta^{-3} + 0.0003\zeta^{-4} - 0.0008\zeta^{-5} + 0.0002\zeta^{-6}) \quad (24)$$

The small-section frozen soil wall conformal mapping function is as follows:

$$z = \omega(\zeta) = 3.5643(\zeta + 0.1493 + 0.0053\zeta^{-1} - 0.0010\zeta^{-2} - 0.0042\zeta^{-3} + 0.0027\zeta^{-4} - 0.0004\zeta^{-5} + 0.0004\zeta^{-6}) \quad (25)$$

4.3. Process of solving for analytical functions based on the FGM model

Given the effect of the steady temperature field on the strength of the frozen soil wall of each layer, when FGM theory is used to calculate the stress on the frozen soil wall of the connecting passage, the frozen soil wall should be considered as a heterogeneous material composed of multiple layers of frozen soil walls with different strengths. Specifically, the frozen soil wall was divided into *n* equal layers along the radial direction, and the centerline temperature of each layer of the frozen soil wall was considered as its temperature (the thickness of the frozen soil wall corresponds to 0 when *n* approaches infinity).

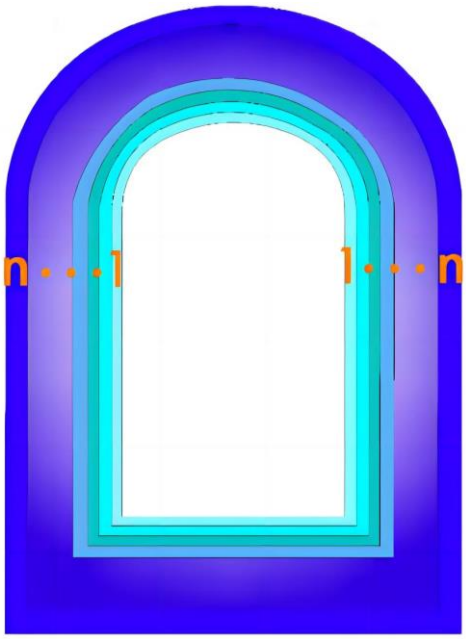

Figure 4. Layers of FGM frozen soil wall.

The temperature field in the region of the frozen soil wall obeys the distribution law of a single-pipe steady temperature field and is expressed as a logarithmic function as follows [30]:

$$T(r) = T_p \frac{ln\frac{R}{R_j}}{ln\frac{R}{r_0}} = 13.5687\, ln\, R_j \tag{26}$$

where T_P denotes the external surface temperature of the freezing pipe, ℃; R denotes the frozen front radius, m; r_0 denotes the radius of the freezing pipe, m; R_j denotes the distance between the centerline of the jth layer of the frozen soil wall and the centerline of the freezing pipe on the Z plane, m.

We assume that the strength of artificial frozen soil is a quadratic function of temperature. Based on studies [35–37] and a geological survey, the quadratic function is fitted as follows:

$$G = -0.0496T^2 - 2.996T + 25 \tag{27}$$

where T denotes the temperature of the frozen soil wall, ℃.

We consider n = 10 as an example the analytic functions for the inner layer in the large-section frozen soil wall are as follows:

$$\begin{cases} \varphi_1(\zeta) = 0.0963\ \zeta^{1} + 0.1573\zeta^{2} + 0.1157\zeta^{-1} + 0.0626\ \zeta^{-2} \\ \psi_1(\zeta) = -0.0663\zeta^{1} + 0.0253\zeta^{2} + 0.3172\zeta^{-1} + 0.0864\zeta^{-2} \end{cases} \tag{28}$$

The analytic functions for the inner layer in the small-section frozen soil wall are as follows:

$$\begin{cases} \varphi_1(\zeta) = 0.0373\zeta^{1} + 0.1149\zeta^{2} + 0.0996\ \zeta^{-1} + 0.0217\zeta^{-2} \\ \psi_1(\zeta) = -0.0313\ \zeta^{1} + 0.0034\ \zeta^{2} + 0.2396\zeta^{-1} + 0.0461^{-2} \end{cases} \tag{29}$$

4.4. Analysis of stress–displacement solutions

By substituting the obtained analytic functions for the inner layer into Eq (8), stress–displacement solutions for each point at the inner boundary of the frozen soil wall after excavation of the connecting passage are obtained. Based on the symmetry of the structure, the boundary of a half section was considered for investigations. According to the coordinate system shown in Figure 1, the vertical axis denotes the starting axis and the counterclockwise direction denotes the positive direction.

4.5. Effect of the number of layers on the stress and displacement of the frozen soil wall

We consider a large-section frozen soil wall as an example the boundary stress and displacement distribution of the frozen soil wall when the freezing pipe is at a distance of l = 1 m from the inner boundary of the centerline and the number of layers cvaries as n = 1, 4, 5, 7, 8, 9, and 10 are shown in Figure 5.

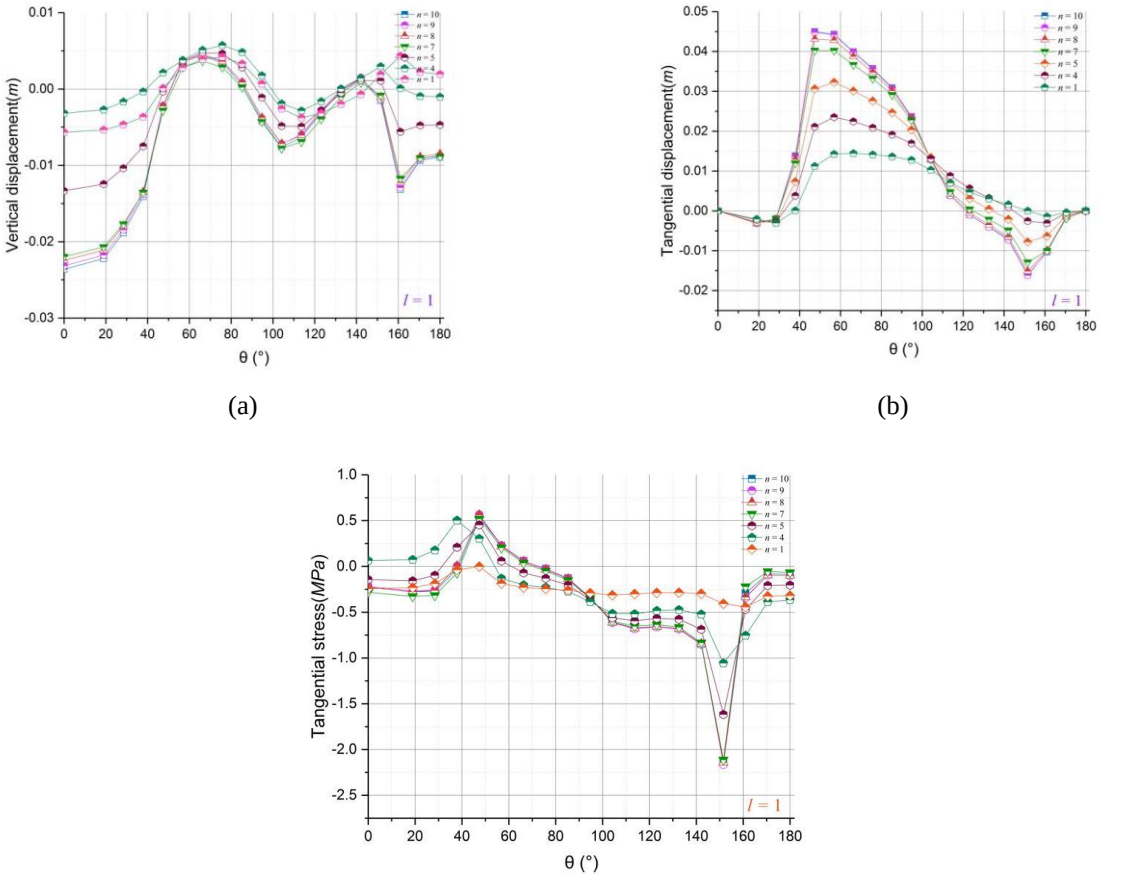

Figure 5. Inner boundary stress and displacement of the FGM frozen soil wall with different layers: (a) Radial displacement of the inner boundary: (b) Tangential displacement of the inner boundary: (c) Tangential stress of the inner boundary.

From the calculation results for the FGM frozen soil wall boundary displacements in and tangential stresses for different numbers of layers, the following observations are concluded:

The frozen soil wall works well as a temporary support structure. The displacements and tangential stresses on the inner boundary of the frozen soil wall are evenly distributed. The maximum tangential stress was mainly distributed near the corner of the inner boundary of the straight wall (θ = 151 °), and this corresponds to 2.37 MPa. The maximum tangential stress was within the maximum compressive strength range of frozen soil at 0°C. However, given the coincidence of the inner boundary with the contour of the excavation and the effect of the excavation, the maximum tangential displacement reached 4.5 cm (located near the arch foot). The result was relatively large, thereby indicating that relying only on the frozen soil wall as a long-term load-bearing structure causes large deformation in the cave.

The frozen soil wall of the large-section connecting passage was narrow and long, the inner boundary was deformed toward the inside of the cavern, and the radial displacement was distributed in an "M" shape. The radial displacement of the dome (θ = 0 °) reached 2.4 cm, which denotes the maximum point of radial displacement of the inner boundary. The radial displacement at the straight wall ($45° \leq \theta \leq 151°$) was small and uniformly distributed (no abrupt change). We used the middle

line (θ = 90°) as the boundary, and reverse deformation occurred on the upper and lower sides. The tunnel floor (151° ≤ θ ≤ 180°) exhibited a slight heave although the maximum radial displacement did not appear at its midpoint (θ = 180°), and it was located on the side closer to the corner of the straight wall.

The tangential displacement of the inner boundary was distributed in an "N" shape, and the tangential displacement of the frozen soil wall on the straight wall significantly exceeded that of the tunnel floor and the arch (0° ≤ θ ≤ 45°). An abrupt change occurred in the tangential displacement near the arch foot (θ = 48°), and the radial displacement small, thereby indicating that the frozen soil on the side of the straight wall exhibited a tendency to sink vertically.

The frozen soil wall was used as a temporary support structure, and its tangential stress (excluding abrupt change points) was negative, thus, it was mainly compressed in the formation. The tangential stress was evenly distributed across the vault, straight wall and floor and were all within 1 MPa. The frozen soil wall at the corner of the inner boundary of the straight wall was partially stretched, thus the tangential stress positive. Unlike the radial displacement, the tangential stress and displacement were significantly affected by the irregularity of the frozen soil wall section form. Abrupt changes occurred in the corner of the straight wall and arch foot. The tangential stress reaches 2.15 MPa, and the tangential displacement reached 4.5 cm.

Yang et al. and Wang [38,39] considered the frozen soil wall of the inclined shaft as a homogeneous model of a frozen soil wall with uniform strength to solve its stress and displacement. The method can be considered as a special solution when the number of layers is n = 1. We compared the calculation results for the homogeneous frozen soil wall model (n = 1) and the FGM model (n = 10), and the results indicate that the displacement and stress calculated by the two are consistent in distribution. Therefore, the distributions of stresses and displacements on the inner boundary of the frozen soil wall were not significantly related to the calculation model (number of layers). The results calculated by using the seven types of layer numbers were similar in terms of the distribution.

The values of the stress and displacement exhibited a significant correlation with the number of layers Given that the strength of the frozen soil wall is affected by the temperature field, the frozen soil wall should be considered as an FGM. The strength of the frozen soil near the freezing pipe increased, and the boundary strength decreased. When the number of frozen soil wall layers increased, the thickness of the frozen soil wall of each layer continued to decrease, and the temperature on the centerline of the frozen soil walls of each layer became increasingly closer to the actual temperature of the frozen soil wall of each layer. Its strength, tangential stress, and displacement should also be closer to the actual values.

The FGM frozen soil wall (n = 10) exhibited a lower overall material strength than the homogeneous frozen soil wall (n = 1). Under the condition of the same ground field, the inner boundary displacements and tangential stresses of the FGM frozen soil wall exceeded those of the homogeneous frozen soil wall, and its distribution of stresses was more concentrated (especially at the corner of the straight wall). This indicates that the design strength of the connecting passage support exceeds that of the homogeneous frozen soil wall when the laminate model of the FGM is used to guide the design of the frozen soil wall. The calculation process for the laminate model is simpler and more in line with the actual engineering case. In order to satisfy the requirements of safe excavation, it is generally necessary to design a lower freezing temperature or a larger frozen soil wall thickness.

It is should be noted that as n increases, the calculation steps also continue to increase. From the aforementioned analysis, when the number of layers corresponds to 10, the calculation results for the displacement and stress on the inner boundary of the frozen soil wall essentially remained stable. When the frozen soil wall is considered as a homogeneous material, the accuracy of its calculation results mainly depends on the actual strength of the frozen soil wall measured at the site, and this varies significantly based on the location of the measurement point.

4.6. Effect of freezing pipe layout position on stress and displacement of frozen soil wall

We consider a large-section frozen soil wall as an example: when the number of layers was n = 10, the inner boundary stress and displacement distributions of the frozen soil wall at distances of l = 0.6, 0.8, 1, 1.2, 1.4, and 1.6 m from the centerline of the freezing pipe shown in Figure 6. The increase in l from 0.6 m to 1.6 m was divided into five equal processes, and the maximum increases in the displacement and tangential stress in the boundary of the frozen soil wall in each process are shown in Figure 7.

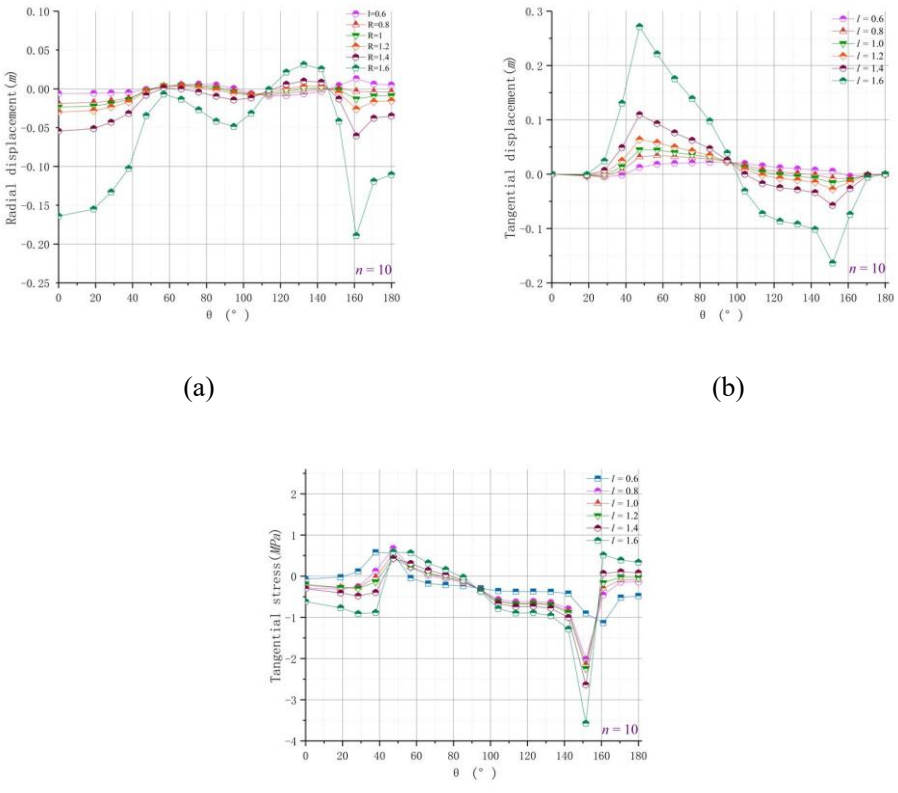

(a) (b)

(c)

Figure 6. Inner boundary stress and displacement results for the FGM frozen soil wall at different freezing pipe positions. (a) Radial displacement of the inner boundary: (b) Tangential displacement of the inner boundary: (c) Tangential stress of the inner boundary.

As shown in Figure 6, although the location of the freezing pipe does not significantly affect the distributions of displacement and tangential stress, it is closely related to the state of the freezing wall force: with increases in the distance between the centerline of the freezing pipe and the inner boundary, the frozen soil wall tensile area moved from $20° \leq \theta \leq 56°$ to the side wall area of $42° \leq \theta \leq 75°$. Simultaneously, the tunnel floor of the frozen soil wall varied from a compressed state to a tensioned state.

We hace combined Figures 6 and 7, and it is observed that the position of the freezing pipe significantly affects the values of the inner boundary displacements and tangential stresses. When the freezing pipe moves, the temperature field in the frozen soil wall region varies, and its stresses and displacements increased differently. Radial displacement was mainly affected by l, and this followed by tangential displacement and tangential stress. It was should be noted that when l = 0.6 m, the inner boundary displacement of the frozen soil wall is close to 0 and the tangential stress distribution is more uniform than in other situations, although the tunnel floor is stretched. When l = 1.6 m, the maximum displacement of the inner boundary exceeds 25 cm and the tangential stress reaches 3.6 MPa (beyond the ultimate compressive strength of frozen soil at 0℃), and this is extremely dangerous. When the inner boundary of the freezing pipe ranged from 0.8 to 1.2 m from the inner boundary, the displacement and tangential stress of the inner boundary were low and theincreases correspond to the lowest (the slope of the curve in Figure 7). Therefore, in an actual engineering case, under the certain freezing temperature, the arrangement of the freezing pipe can be appropriately adjusted to improve the stability factor of the inner boundary for the freezing wall during excavation.

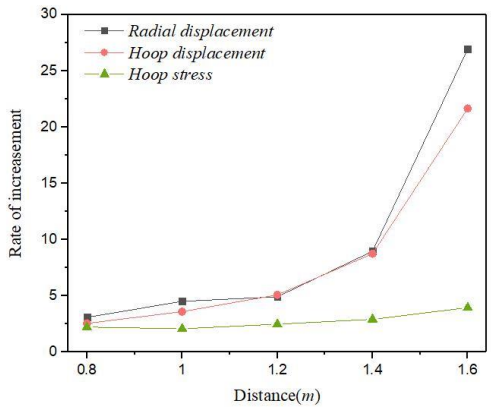

Figure 7. Maximum increase in inner boundary displacement and stress of FGM frozen soil walls in each process.

4.7. Stress and displacement of frozen soil walls with large and small sections

The distributions of stresses and displacements at the inner and outer boundaries of large and small sections are shown below:

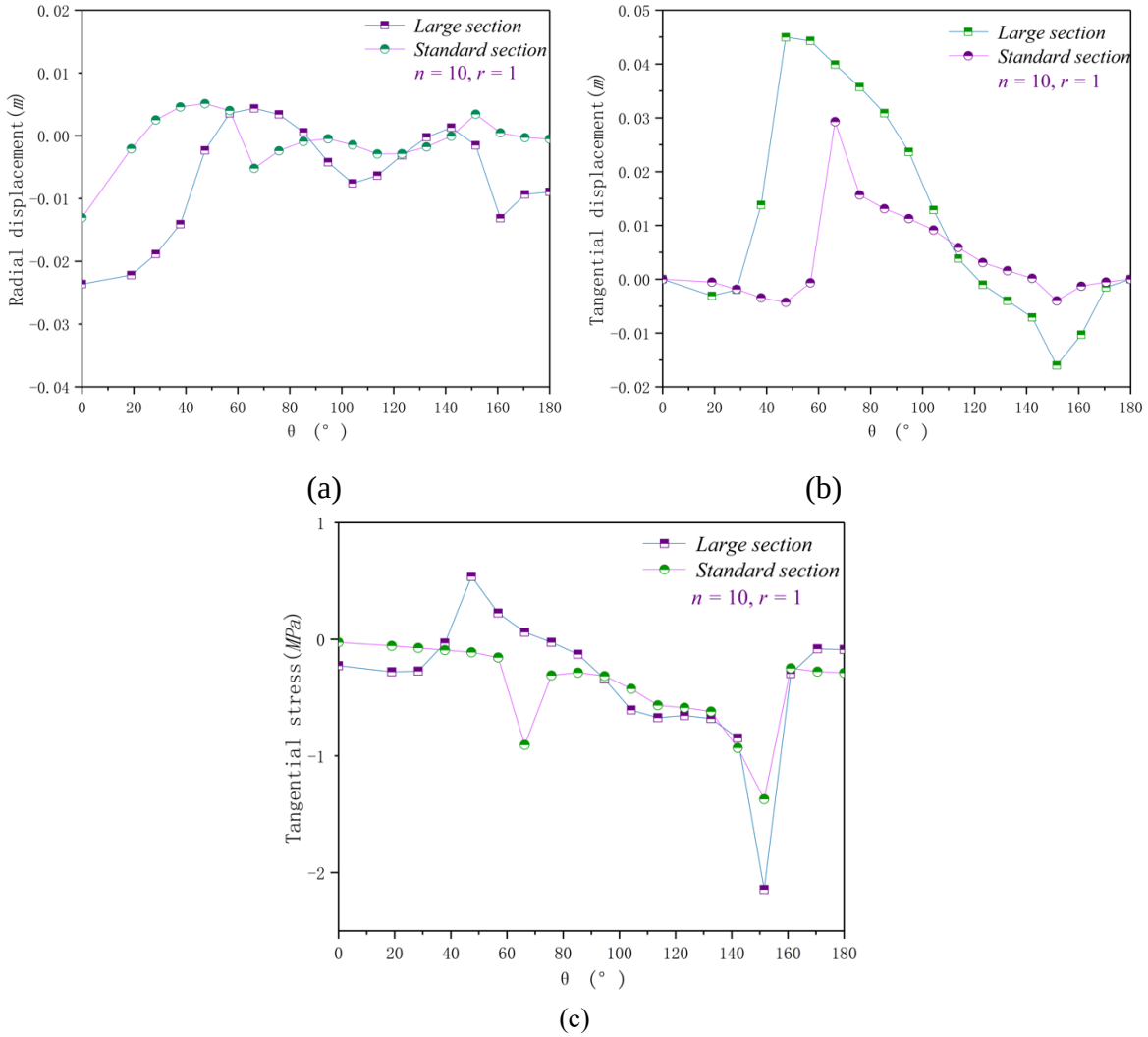

Figure 8. Inner boundary stress and displacement of the FGM frozen soil wall of an actual engineering case: (a) Radial displacement of the inner boundary: (b) Tangential displacement of the inner boundary: (c) Tangential stress of the inner boundary.

As shown in Figure 8, a change in the section changes the distributions of stress and displacement of the frozen soil wall. The two sections were not similar (the large section can be considered as the result of the "stretching" of the small section straight wall); thus, there is a certain difference between the central angle corresponding to the arch foot and corner of straight wall, thereby resulting in a certain linearly proportional relationship between the tangential displacement of the two sections with the increase of the central angle. Generally, the arch ($0° \leq \theta \leq 71°$) and floor ($138° \leq \theta \leq 180°$) of the small-section frozen soil wall are mainly deformed toward the outside of the cave, and the deformation at the straight wall is low.

The stress of the small-section frozen soil wall exceeded that of the large-section frozen soil wall. The radial displacement of the large-section frozen soil wall in the vault and floor was approximately 1 cm higher than that of the small section with the same design parameters. The tensile strength of frozen soil was significantly lower than the compressive strength; thus, the situation should be avoided. In comparison to the two sections, the tangential stress on the frozen soil

wall in the small-section form is negative. The straight wall was not stretched, and the abrupt degree of tangential stress was relatively low, i.e., the stress distribution was more uniform. When designing a large-section frozen soil wall, the freezing pipe temperature at the corner of the straight wall can be appropriately reduced to increase the excavation safety factor.

5. Analysis of the numerical method

5.1. Numerical simulation

Numerical stimulation with FLAC^{3D} was used to compare the stress and displacement on the homogeneous frozen soil wall (n = 1) and FGM frozen soil wall (n = 10) after the excavation of the connecting passage. An elastic–plastic model with the Mohr–Coulomb failure criterion was employed for the soil in the 3D model. The frozen soil wall was simplified as an elastic material, and the surrounding rock-mass was simplified as a Mohr–Coulomb material. The mechanical parameters of the soils and frozen soil wall used in the FLAC^{3D} simulation are listed in Tables 1 and 2 and were derived from geological investigation and in-situ measurement. The layout of the numerical model is shown in Figure 9, and the stress–displacement results was shown in Figure 10. The homogeneous frozen soil wall (n = 1) and FGM frozen soil wall (n = 10) were unloaded and simulated. The Mohr–Coulomb constitutive structure was adopted for the formation (see Tables 1 and 2 for parameters, Figure 9 for the schematic model, and Figure 10 for the calculation results). Regarding the FGM frozen soil wall simulation, based on the design, the frozen soil wall of the connecting passagewas divided into 10 equal layers along the thickness direction, and the strength parameters each frozen soil wall layer were modified by the results calculated by using Eqs (27) and (28).

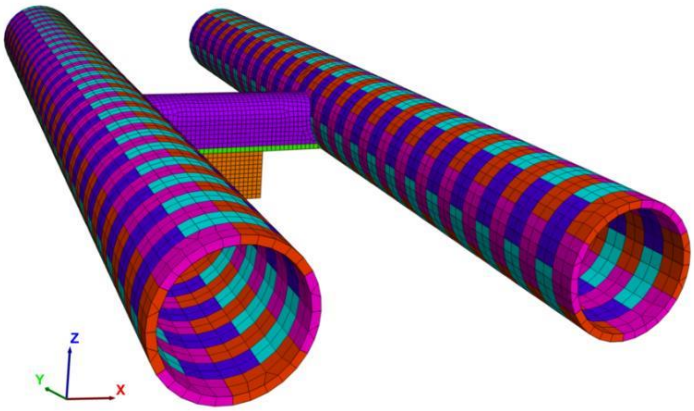

Figure 9. Numerical simulation model: shield tunnel and connecting passage.

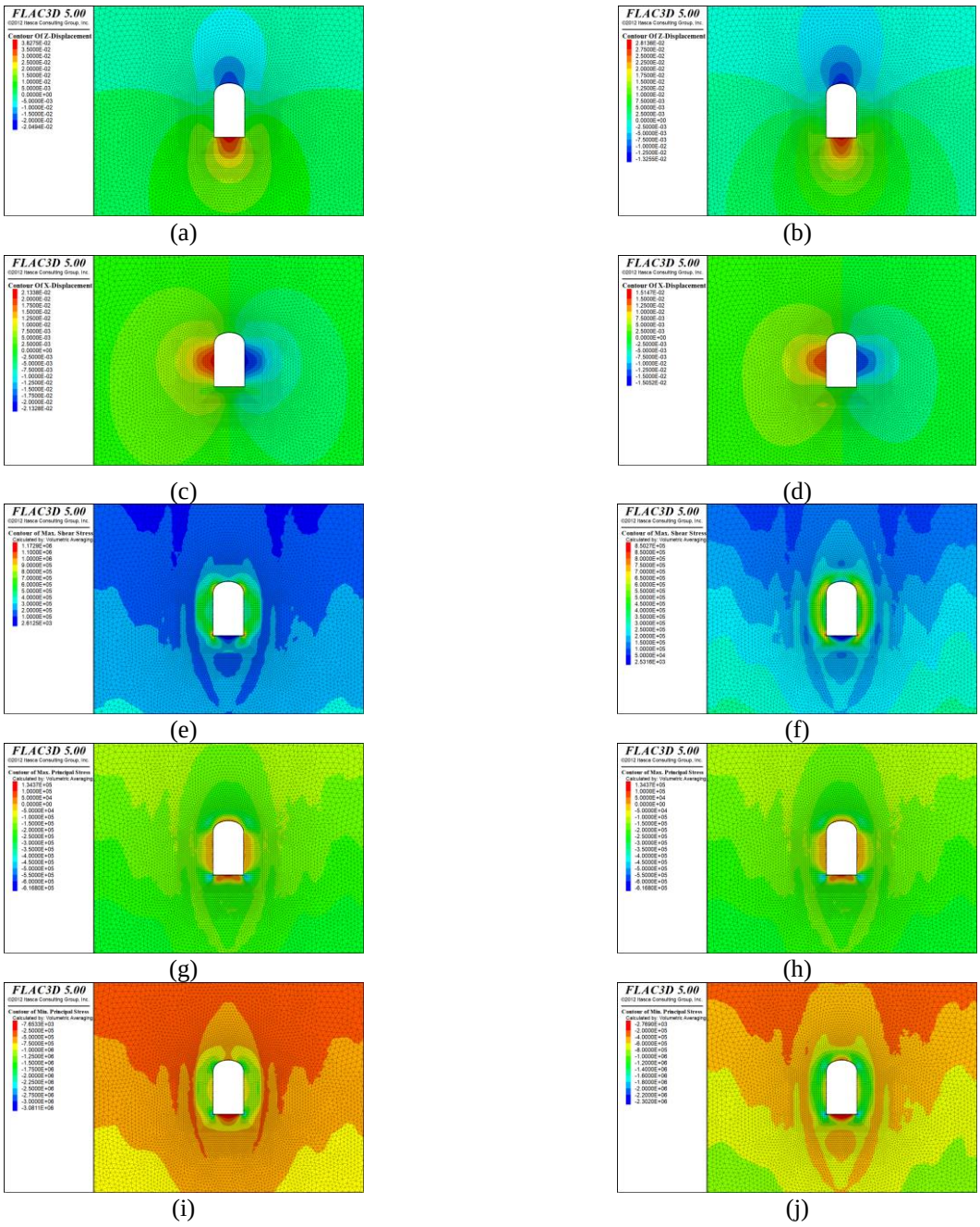

Figure 10. Numerical simulation solutions for the frozen soil wall from different material models: (a) Vertical displacement of the FGM frozen soil wall: (b) Vertical displacement of the homogeneous frozen soil wall: (c) Lateral displacement of the FGM frozen soil wall: (d) Lateral displacement of the homogeneous frozen soil wall: (e) Maximum shear stress of the FGM frozen soil wall: (f) Maximum shear stress of the homogeneous frozen soil wall: (g) Maximum principal stress of the FGM frozen soil wall: (h) Maximum principal stress of the homogeneous frozen soil wall: (i) Minimum principal stress of the FGM frozen soil wall: (j) Minimum principal stress of the homogeneous frozen soil wall.

5.2. Comparison of analytical and numerical results

Yang et al. [40] conducted numerical simulations of frost heave with coupled water freezing, temperature and stress fields in tunnel excavation. The formation passing through was considered as silty sand, of which the properties were similar to the site investigation discussed in this paper (Table 1). Besides, because the position of freezing pipes in Yang's engineering case was setup in the same was as in this paper, both the published numerical and theoretical results were adopted to enbale comparison with those calculated in this paper (Figure 11).

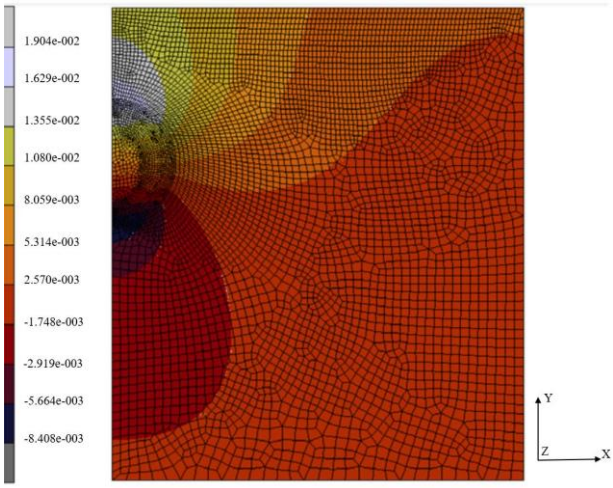

Figure 11. Contours of frost heave: vertical displacements (form Yang et al. [40]).

The vertical displacement, one of the most important considerations, should be compared carefully. Thus the displacements around the connecting passage were obtained from the results shown in Figure 11. Following that, Figure 12 shows the calculated displacements as the angle θ varies.

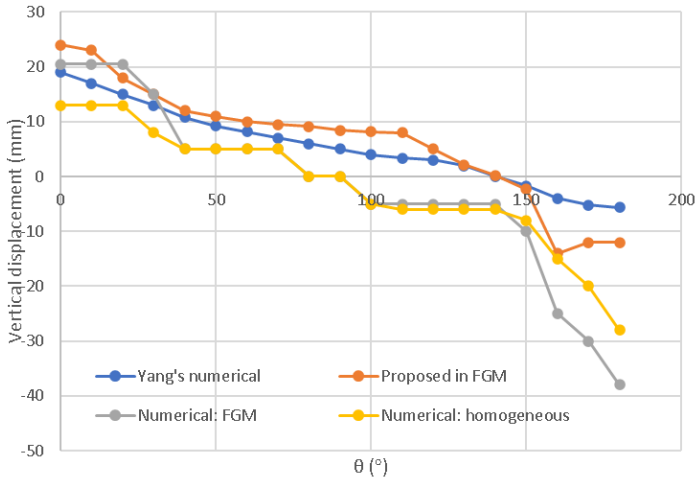

Figure 12. Comparison of numerical data and published results.

It can be seen that the trend of vertical displacements is similar as θ changes, which to some extent verifies the correctness of the proposed functions. The numerical results in this paper are evidently larger than those of the other three: as far as the authors are aware, the bottom material mentioned in the passage may be inaccurate. However, this will not influence the vertical displacement at the top of arch. As shown in Figure 12, the vertical displacement is quite close when it comes tothe FGM model. We could say the proposed function considering the material can predict the deformation of frozen soil and also be a bit conservative.

As shown in Figure 10, the analytical solution of the boundary stress and displacement of the frozen soil wall obtained based on the mechanical model of the FGM frozen soil wall was similar to the numerical solution. With respect to the distribution, the stress distributions of the FGM frozen soil wall and homogeneous frozen soil wall were identical to the displacement distribution, and the stress concentration is evident at the arch foot and the corner of the straight wall. Additionally, as compared with the outer boundary, the inner boundary of the frozen soil wall is more significantly affected by excavation, and the stress and displacement exhibited a decreasing trend along the radius of the frozen soil wall. This indicates that the stress and displacement on the inner boundary of the frozen soil wall are suitable for the mechanical analysis of the frozen soil wall. With respect to the values of stress and displacement for the numerical method, given the same ground stress field, the stress and displacement on the inner boundary increased significantly more than those on the homogeneous frozen soil wall after considering the FGM characteristics of the frozen soil wall. This indicates that the results of the analytical solutions are reliable.

6. Conclusions

In the study, the effects of the number of layers, the position of the freezing pipe, and the shape of the section on the stability of the frozen soil wall have been analyzed via the complex variable function method. Specific conclusions include the following:

1) Given the relationship between the strength of the frozen soil wall and the steady temperature field, a mechanical model of the frozen soil wall of the connecting passage based on an FGM was proposed, and the boundary stress and displacement of the frozen soil wall of the heterogeneous connecting passage (straight-arch wall) were solved by employing a laminate model of an FGM and the complex variable function method.

2) We compared the mechanical behavior of the two sections of a frozen soil wall in a supporting project and observed that the frozen soil wall of the connecting passage in the actual engineering case (as a temporary support structure) effectively maintained the stability of the cave after excavation. The decrease in the aspect ratio of the frozen soil wall reduced the inner boundary displacement and tangential stress and also resulted in the redistribution of the stress and displacement. Aa compared to the large-section frozen soil wall, the small-section frozen soil wall to be more uniform in the distributions of displacement and tangential stress.

3) As a heterogeneous material, the frozen soil wall of the metro line connecting passage exhibited FGM characteristics, and the number of layers significantly affected the values of the boundary displacement and tangential stress of the frozen soil wall. When the number of layersincreased, the displacement and stress of the inner boundary increased correspondingly and were closer to an actual values.

4) The values of the inner boundary displacement , tangential stress and the stress characteristics and the effect of the frozen soil wall are also very significant at the position of the freezing pipe. When the center line of the freezing pipe moved to the outer boundary, the tension zone of the frozen soil wall began to shift and the displacement and tangential stress of the inner boundary continuously increased. In practice, the center line position of the freezing pipe can be adjusted within the range of 0.8 m to 1.2 m to improve the stability of the inner boundary of the freezing wall after excavation.

It should be noted that although the mechanical model of the frozen soil wall proposed in the paper establishes the link between the mechanical behavior analysis of the frozen soil wall and steady temperature field, the conditions considered are relatively simple and exhibit certain limitations. In an actual engineering case, the temperature field in the frozen soil region is complex and variable, and this is closely related to the variation of freezing pipe arrangement, freezing time span, freezing temperature, and the thermal parameters of formation among others. Simultaneously, the stress of the metro line connecting passage is a typical 3D problem, and the excavation method and timing of the interval tunnel and the connecting passage significantly affect stress.

Use of AI tools declaration

The authors declare that they have not used artificial intelligence tools in the creation of this article.

Acknowledgement

This research was funded by the Science and Technology Project of the Department of Transportation of Yunnan Province (No. YJKJ[2019]59). The authors appreciatively acknowledge the financial support of the above-mentioned agency.

Conflicts of Interest

The authors declare that they have no conflicts of interest.

References

1. T. Tsutomu, S. Kiriyama, T. Kato, Jointing of two tunnel shields using artificial underground freezing, *Dev. Geotech. Eng.*, **13** (1979), 519–529. https://doi.org/10.1016/0013-7952(79)90054-1
2. H. L. Jessberger, Theory and application of ground freezing in civil engineering, *Cold Reg. Sci. Technol.*, **3** (1980), 3–27. https://doi.org/10.1016/0165-232X(80)90003-8
3. X. S. Chen, Ground Freezing Method, *Beijing: people's communications press*, 2013.
4. H. Ding, F. Z. Li, H. Cui, Three-Dimensional Numerical Analysis on Freezing Temperature Field in Subway Cross-Passage, *Mine Constr. Technol.*, **39** (2018), 54–57. https://doi.org/10.19458/j.cnki.cn11-2456/td.2018.01.013
5. X. M. Zhou, M. S. Wang, L. G. Tao, Model test and prototype observation on artificial ground freezing and tunneling of Beijing subway, *Chin. J. Geotech. Eng.*, **25** (2003), 676–679. https://doi.org/CNKI:SUN:YTGC.0.2003-06-006

6. X. Hu, T. Fang, J. Chen, H. Ren, W. Guo, A large-scale physical model test on frozen status in freeze-sealing pipe roof method for tunnel construction, *Tunnelling Underground Space Technol.*, **72** (2018), 55–63. https://doi.org/10.1016/j.tust.2017.10.004
7. F. T. Yue, P. Y. Qiu, G. X. Yang, G. X. Yang, R. J. Shi, Design and practice of freezing method applied to connected aisle in tunnel under complex conditions, *Chin. J. Geotech. Eng.*, **28** (2006), 660–663. https://doi.org/10.1016/S1872-1508(06)60035-1
8. I. S. Sokolnikoff, Mathematical theory of elasticity, *New York: McGraw-Hill*, 1956.
9. V. G. Ukadgaonker, P. Awasare, A novel method of stress analysis of an infinite plate with rounded corners of a rectangular hole under uniform edge loading, *Indian J. Eng. Materialsences*, **1** (1994), 17–25. https://doi.org/10.1109/96.296440
10. K. R. Y. Simha, S. S. Mohapatra, Stress concentration around irregular holes using complex variable method, *Sadhana*, **23** (1998), 393–412. https://doi.org/10.1007/BF02745750
11. D. S. Sharma, Stress distribution around polygonal hole, *Int. J. Mech. Sci.*, **65** (2012), 115–124. https://doi.org/10.1016/j.ijmecsci.2012.09.009
12. Z. M. Chen, Analytical method for mechanical analysis of surrounding rock, *China Coal Industry Publishing House*, 1994.
13. G. E. Exadaktylos, M. C. Stavropoulou, A closed-form elastic solution for stresses and displacements around tunnels, *Int. J. Rock Mech. Mining Sci.*, **39** (2002), 905–916. https://doi.org/10.1016/S1365-1609(02)00079-5
14. G. E. Exadaktylos, P. A. Liolios, M. C. Stavropoulou, A semi-analytical elastic stress–displacement solution for notched circular openings in rocks, *Int. J. Solids Struct.*, **40** (2003), 1165–1187. https://doi.org/10.1016/S0020-7683(02)00646-7
15. P. Li, J. Liu, F. Su, X. Li, Analytical continuation method for solving stress and displacement of surrounding rock buried tunnel excavation with arbitrary shape section, *J. Tongji Univ.*, **41** (2013), 1483–1489. https://doi.org/10.3969/j.issn.0253-374x.2013.10.006
16. Q. Cheng, A. Lu, C. Yin, Analytical stress solutions for a deep buried circular tunnel under an unsteady temperature field, *Rock Mech. Rock Eng.*, **54** (2021), 1355–1368. https://doi.org/10.1007/s00603-020-02316-8
17. A. Z. Lu, L. Q. Zhang, Complex function method for mechanical analysis of underground tunnel, *China Science Press*, 2007.
18. A. Z. Lu, N. Zhang, L. Kuang, Analytic solutions of stress and displacement for a non-circular tunnel at great depth including support delay, *Int. J. Rock Mech. Mining Sci.*, **70** (2014), 69–81. https://doi.org/10.1016/j.ijrmms.2014.04.008
19. A. Z. Lu, N. Zhang, Y. Qin, Analytical solutions for the stress of a lined non-circular tunnel under full-slip contact conditions, *Int. J. Rock Mech. Mining Sci.*, **79** (2015), 183–192. https://doi.org/10.1016/j.ijrmms.2015.08.008
20. A. Z. Lu, N. Zhang, S. J. Wang, X. L. Zhang, Analytical solution for a lined tunnel with arbitrary cross sections excavated in orthogonal anisotropic rock mass, *Int. J. Geomech.*, **17** (2017). https://doi.org/10.1061/(ASCE)GM.1943-5622.0000912
21. N. Tutuncu, M. Ozturk, Exact solutions for stresses in functionally graded pressure vessels, *Compos. Part B Eng.*, **32** (2001), 683–686. https://doi.org/10.1016/S1359-8368(01)00041-5
22. T. Akis, A. N. Eraslan, The stress response and onset of yield of rotating FGM hollow shafts, *Acta Mech.*, **187** (2006), 169–187. https://doi.org/10.1007/s00707-006-0374-z

23. Y. Z. Chen, X. Y. Lin, Elastic analysis for thick cylinders and spherical pressure vessels made of functionally graded materials, *Comput. Mater. Sci.*, **44** (2008), 581–587. https://doi.org/10.1016/j.commatsci.2008.04.018
24. P. Das, M. A. Islam, S. Somadder, M. A. Hasib, Analytical and numerical analysis of functionally graded (FGM) axisymmetric cylinders under thermo-mechanical loadings, *Mater. Today Commun.*, **33** (2022), 104405. https://doi.org/10.1016/j.mtcomm.2022.104405
25. C. G. Zhang, B. X. Gao, T. B. Li, Z. P. Shan, An elastic-plastic solution for frost heaving force of cold region tunnels considering transversely isotropic frost heave and displacement release, *Rock Soil Mech.*, **42** (2021), 2967–2976. https://doi.org/10.16285/j.rsm.2021.0635
26. Z. Y. Guo, H. N. Wang, M. J. Jiang, Elastoplastic analytical investigation of wellbore stability for drilling in methane hydrate-bearing sediments, *J. Nat. Gas Sci. Eng.*, **79** (2020), 103344. https://doi.org/10.1016/j.jngse.2020.103344
27. X. Y. Cao, J. H. Zhao, C. G. Zhang, Elastoplastic stress analysis of frozen soil wall based on unified strength theory, *Rock Soil Mech.*, **38** (2017), 769–774. https://doi.org/10.16285/j.rsm.2017.03.020
28. X. D. Hu, Y. Wang, Analytical solution of three-row-piped frozen temperature field by means of superposition of potential function, *Chin. J. Rock Mech. Eng.*, **31** (2012), 1071–1080.
29. X. D. Hu, S. Chang, Stress field analysis of functionally graded material frozen soil wall in doublerow-pipe shaft freezing, *Eng. Mech.*, **31** (2014), 145–153. https://doi.org/10.6052/j.issn.1000-4750.2012.09.0651
30. L. Xiang, F. Ye, X. Liang, Multi-tube freezing temperature field considering range of influence of freezing tubes, *Tunnel Constr.*, **41** (2021), 52–59.
31. Z. M. Chen, Analytical method for mechanical analysis of surrounding rock, *China Coal Industry Publishing House*, 1994.
32. J. Dryden, K. Jayaraman, Effect of Inhomogeneity on the Stress in Pipes, *J. Elasticity*, **83** (2006), 179–189. https://doi.org/10.1007/s10659-005-9043-z
33. M. Mohammadi, J. R. Dryden, Influence of the spatial variation of Poisson's ratio upon the elastic field in nonhomogeneous axisymmetric bodies, *Int. J. Solids Struct.*, **46** (2009), 788–795. https://doi.org/10.1016/j.ijsolstr.2008.09.030
34. M. Mohammadi, J. R. Dryden, L. Y. Jiang, Stress concentration around a hole in a radially inhomogeneous plate, *Int. J. Solids Struct.*, **48** (2011), 83–491. https://doi.org/10.1016/j.ijsolstr.2010.10.013
35. Z. W. Wu, W. Ma, C. Q. Zhang, L. Y. Jiang, Strength characteristics of frozen sandy soil, *J. Glaciol. Geol.*, **16** (1994), 15–20. https://doi.org/10.13247/j.cnki.jcumt.000611
36. G. M. Xi, G. S. Yang, L. Pang, X. T. Lv, L. Fang, Experimental study on basic mechanical behaviors of sandy mudstone under low freezing temperature, *J. China Coal Soc.*, **39** (2014), 1262–1268. https://doi.org/10.13225/j.cnki.jccs.2014.0533
37. G. S. Yang, Y. Wei, Y. J. Shen, L. Wang, H. Liu, X. H. Dong, et al., Mechanical behavior and strength forecast model of frozen saturated sandstone under triaxial compression, *Chin. J. Rock Mech. Eng.*, **38** (2019), 683–694. https://doi.org/10.13722/j.cnki.jrme.2018.1417
38. R. S. Yang, Q. X. Wang, S. Z. Chen, Elastic analysis of irregular inclined shaft lining subjected to water pressure, *J. China Univ. Mining Technol.*, **46** (2017), 48–57. https://doi.org/10.13247/j.cnki.jcumt.000611

39. Q. X. Wang, Research on deformation law and design method of inclined shaft frozen wall, *China University of Mining and Technology*, 2017.
40. P. Yang, J. M. Ke, J. G. Wang, Y. K. Chow, F. B. Zhu, Numerical simulation of frost heave with coupled water freezing, temperature and stress fields in tunnel excavation, *Comput. Geotech.*, **33** (2006), 330–340. https://doi.org/10.1016/j.compgeo.2006.07.006

AIMS Press